Chemical Engineering Journal 143 (2008) 186–194

Contents lists available at ScienceDirect

Chemical Engineering Journal

journal homepage: www.elsevier.com/locate/cej

Synthesis of nanocarbons via ethanol dry reforming over a carbon steel catalyst

Jasmin Blanchard, Hicham Oudghiri-Hassani, Nicolas Abatzoglou*, Sepideh Jankhah, François Gitzhofer

Department of Chemical Engineering, Université de Sherbrooke, Sherbrooke, Quebec, Canada

ARTICLE INFO

Article history:
Received 13 September 2007
Received in revised form 29 March 2008
Accepted 10 April 2008

Keywords:
Dry reforming
Ethanol
Catalyst
Steel
CO_2 sequestration
Carbon nanofilaments (CNF)
FEG
XRD

ABSTRACT

In previous publications it was shown that carbon steel is an effective ethanol dry reforming catalyst, if carbon nanofilaments (CNF) constitute a desired product of the reaction. The objective of the present work was to investigate this catalytic reaction step and to present data on CNF and other reaction products as a function of catalyst nature and preparation as well as of experimental conditions.

The methodology included 2 experimental set-ups: a bench-scale, fixed-bed reactor equipped with an on-line gas chromatograph for exit gas analysis and a differential reactor. Field emission gun scanning electron microscopy and X-ray diffraction analyses were used to characterize catalyst surface and CNF.

The results showed that the formation of micro- and nanoparticles of magnetite on the steel surface was a necessary step for the activation and enhancement of its catalytic properties. The so-activated catalyst reformed ethanol with CO_2 into H_2, CO, H_2O and CNF, via the formation of iron carbide particles (Fe_3C). These iron carbide particles were derived from magnetite particles, via reduction and carbon sequestration reactions, and were the basis for catalytic CNF production.

1. Introduction

Since Iijima's original work [1], carbon nanotubes (CNT) have been recognized as a material with promising potential applications in chemistry and physics. Several methods have been developed to synthesize them. However, synthesis by an arc-discharge process, between 2 graphite electrodes [2], has historically been the most widely used; other processes, such as laser ablation [3] and catalytic decomposition of molecules containing carbon [4], have also been tested. CNT can also be obtained by the electrochemical route with graphite electrodes immersed in a molten salt medium [5,6], by graphite vaporization–condensation employing solar energy (catalyzed by Co and Ni) [7], or by hydrocarbon pyrolysis, which is closer to the work presented in this paper. It is important to define carbon nanofilaments (CNF) and CNT. The difference between CNF and CNT is the orientation of their constitutive graphite layers relative to the axis of their cylindrical form. Nanotubes are composed of concentric graphite layers (cylinders); thus, the layers are parallel to the axis. Nanofilament structure is made of layers perpendicular or oblique to the graphite axis; thus, there are planar perpendicular sheets and tilted, winding sheets with conical shapes [8].

The production of nanotubes by hydrocarbon pyrolysis, at temperatures typically above 600 °C, has been studied in the presence of various catalysts: metals (Co, Ni, Fe, Pt, Cu, Pd) and their alloys, and deposited in the form of nanoparticles on a substrate [8]. Narkiewicz et al. [9] prepared their catalysts by depositing iron powder at a ceramic support (6% w/w), followed by oxidative atmosphere treatment. The required catalyst particles were obtained via reductive treatment applied to intermediate iron oxide. Another route was the deposition of iron oxides on alumina or silica substrates from a precursor, such as an ethanol solution of $Fe(NO)_3$ [10]. Vaporized metallocenes (ferrocene, cobaltocene or nickelocene), either alone or with a hydrocarbon, are variants of the process [11,12]. In all these cases, the nanotubes are formed on metal particles. Almost any kind of hydrocarbon can be used, i.e., methane, acetylene [13], benzene [13] or camphor ($C_{10}H_{16}O$) [12]. At temperatures above 1000 °C, it has been reported that the chemical structure of the hydrocarbon only slightly influences the results of hydrocarbon pyrolysis [13], while reaction space velocity and local temperature play the most important roles [14]. The nanotube and filament growth mechanism, proposed some 30 years ago, still prevails today [2,15,16]. According to this mechanism, aggregated carbon, being less organized than filaments and nanotubes, is initially absorbed on one side of a carbide particle. The carbon diffuses through the particle and emerges at the opposite side, forming layers of well-ordered graphitic carbon. Another proposed mechanism involves the growth of nanotubes from catalyst grains (particles) on a ceramic support or single catalyst grains [17].

* Corresponding author at: 2500 boul. Université, Sherbrooke, Québec, Canada J1K 2R1. Tel.: +1 819 821 7904; fax: +1 819 821 7955.
E-mail address: Nicolas.Abatzoglou@USherbrooke.ca (N. Abatzoglou).

1385-8947/$ – see front matter © 2008 Elsevier B.V. All rights reserved.
doi:10.1016/j.cej.2008.04.012

The exact mechanism depends on many parameters, such as catalyst composition, the precursor hydrocarbon used, reactor temperature, geometric aspects, such as particle size, carrier gas composition and its ratio to the carried gas [8,18]. Some gases deployed were acetylene [16,19], methane [20–22], CO [14,21,23–25] and acetone [26]. In a recently accepted paper of the authors, it has been shown that nanofilaments carrying nanograins of iron carbides have similar catalytic activities for CNF production and that these carbides are in the catalytically active phase. However, since no significant change in the size and morphology of these grains has been observed, the mechanism is rather unclear, so that additional work is needed to better understand it.

The effects of the catalysts (metals, alloys and supports) on filament properties and carbon deposition yield have also been studied [27]: supports: graphite vs. Si [19,28], alloys: Fe–Cu [28,29], Fe–Ni [30], and metals: Co, Cr [19,24], Cu, Ni, Ag [24], Rh [31], V, Mo [24,32], as well as iron compounds [14,20,24,25,33]. The impact of particle shape on filament structure also has been investigated [27,34]. Besides, the production and co-existence of various types of carbon within a given reaction environment indicate that different reaction mechanisms can co-exist. Iron carbides are well-known compounds for the filament production via hydrocarbon and CO decomposition [14,21,23].

Catalytic reforming of ethanol, as reported in the literature, has been undertaken with steam, employing metal particles supported on a ceramic matrix. The metals studied were Rh [17,35,36], Ru, Pd, Pt [17], Ni [37,38], Cu [39] and Co [38,40]. The supports were Al_2O_3 [17,39], MgO [17,37,38], TiO_2, SiO_2 [17] and ZrO_2–CeO_2 [36]. In these experiments, the catalyst for ethanol reforming was composed of a metal deposited as nano- or microparticles on a ceramic substrate. The main concern over ethanol reforming, as with almost all hydrocarbon reforming, is to limit the carbon formation that traps and generally decreases catalytically active sites or otherwise harms the catalyst's structural integrity. Reaction temperature, the ratio of ethanol or hydrocarbons to H_2O and the composition of the catalyst, are the main parameters influencing carbon formation. In industrial hydrocarbon reforming processes, low temperatures, close stoichiometric ratios and low carbon formation are desirable. Most studies reported in the literature have focused on improving catalyst formulation towards this direction. Carbon formation occurs readily on ferromagnetic metals (Fe, Co and Ni), principally via the Boudouard reaction [14,41]. Multivalent iron oxides, such as magnetite, are well-known catalysts for the Boudouard reaction [20].

The best way to avoid carbon deactivation is to choose a catalyst that is not considerably disturbed by carbon accumulation. Nickel strips have been tested in a similar manner with acetone at 487 °C. Oxidative-reduction treatment at high temperature prior to the reaction enhances the specific surface, and the carbon obtained is partially in the form of CNF [26]. Unfortunately, this catalyst is reported to lose much of its activity in 1 h because of carbon accumulation. Another group [33] investigated iron based metal strips to decompose acetylene at 750 °C and produce carbon filaments. They found that FeO was the most active catalyst (it acts as a precursor to increase the Fe surface in situ), whereas cementite is not active [33]. In another laboratory, iron powder (obtained from the reduction of an iron oxide) was used to catalyze CNF production from a mixture of $CO/3H_2$ at 680 °C [42]. In 2 min, all the iron was transformed to cementite, which appeared to be the catalytically active phase, and CNF began to grow after 10 min. A 1983 study [20] reported that stainless steel 304 tubes can efficiently form carbon fibres of 10 μm average diameter at high temperature from hydrocarbon pyrolysis. The gas utilized in this work was industrial methane, and the reaction temperature was varied between 950 and 1075 °C. In 2004, Pan et al. [44] investigated the production of CNF and CNT with ethanol. Pure ethanol was burned in a flame, and a substrate (Ni alloy or stainless steel 304 plate treated with nitric acid to produce small oxide particles on the surface) was introduced into the flame.

In comparison to noble metals, steel is both cheap and sufficiently active to reform hydrocarbons with a simple 2D sheet, compared to the 3D "sponge-like" material normally employed as catalyst. Previous work [45–47] has shown that stainless and carbon steels are both efficient reforming catalysts for ethanol. These researchers proved that a simple, iron-based, non-porous catalytic formulation allows CNF production during dry reforming, without harming catalytic properties. The reaction takes place at the expense of iron catalysts, which are consumed as nanograins inside the CNF, but this is not of significant concern because of the low cost of the catalytic material used. The same authors have also demonstrated that the reforming catalytic properties of these iron-based formulations are not available before their thermal pretreatment. A review of the literature has revealed that there is a relatively rich reporting of studies on the thermal treatment of carbon steels under various reactive atmospheres (O_2, CO_2 or H_2O plus an inert constituent) [48,49].

Thus, thermal treatment (at temperatures above 400 °C) of steel, under a mixture of nitrogen and oxygen, results in the formation of a film of iron oxides at the surfaces of the steel form. Temperature, oxygen concentration and post-reaction cooling rate are the principal parameters that influence the rate of film formation and the type(s) of oxides formed (principally wüstite (FeO), magnetite (Fe_3O_4, a spinel), and hematite (Fe_2O_3)) [43,48,50]. If formed at a temperature above 700 °C, the oxide film is made up of 3 layers: a thick one directly attached to the steel surface and composed of wüstite; a thinner intermediate one, comprised of magnetite; and an even thinner one, of hematite [43,50]. The oxide layer's thickness can vary between a few μm and a few mm [43], depending on the conditions/circumstances of their formation. The unequal diffusion coefficients for iron through the oxide layers are the principal reason for the differences in thickness of the various oxide layers. For reaction temperatures below 700 °C, the sample preparation method also greatly influences the type of oxides formed and the thickness ratio of the different layers [43,49]. At temperatures below 570 °C, the wüstite layer is not normally formed because it is thermodynamically less stable than the other possible oxides [43]. For temperatures below 550 °C, sample preparation (like cold "working") is a significant parameter affecting the oxidation rate [43,51].

A recently published paper of the authors [52] demonstrates the use of iron carbide for ethanol reforming with CO_2 to produce CNF. One patent claims the reforming of various alcohols, but water is added only as a means of adjusting the H_2/CO ratio, and CO_2 is considered as inert [53].

The present work describes a process involving CO_2 to reform ethanol to H_2 and CO and to "sequester" at least a part of the CO_2 (an important greenhouse gas) under the form of CNF and MWNTs (multi-walled nanotubes). In previous published works by the authors [45–47], it has been shown that a sheet of common carbon steel is able to produce CNF after pretreatment activation, but no data were available then regarding the prevailing mechanism of the phenomenon. The process has been studied by gas chromatography (GC) and mass spectrometry as well as by diagnostic methods for CNF synthesized and catalysts used, such as transmission electron microscopy (TEM), field emission gun scanning electron microscopy (FEGSEM) and X-ray diffraction (XRD). It has been reported that initial catalytic activity is mainly due to the presence of the oxidized states of iron and that subsequent reduction of the latter leads to the formation of carbides thought to be the

precursors of MWNTs. The overall targeted reaction is as follows:

$$3C_2H_5OH + CO_2 \leftrightarrow 5CO + 9H_2 + 2C \quad (1)$$

The carbon formed during catalytic reforming takes various forms (graphitic, resinous, coal-like, filamental and nanotube). Preconditioning of the catalyst is vital to obtain satisfactory product purity and homogeneity. The magnitudes of the reforming parameters (temperature, residence time, particle size) also significantly affect the form of the deposited carbon [27,41].

2. Experimental details

2.1. Chemicals

Reactant gases were used as supplied by Praxair. Purity was 99.996% v/v for CO_2 and 99.9999% v/v for Ar. Ethanol, obtained from Commercial Alcohols Inc., had a purity of 99.9% v/v.

2.2. The catalysts

The non-porous (2D) catalysts studied in this work were: (1) Carbon steel 1008 plate procured from Technologie Supérieure d'Alliages, and (2) "Shim" steel AISI 1010 from the Precision Brand Company. The carbon steel had 0.06% C, and a Mn impurity of 0.29%, plus traces (total of around 0.23%) of P, S, Cu, Ni, Cr, Nb, Mo, N, Sn and Ti. However, shim steel contained a maximum of 0.13% C, 0.3–0.6% Mn, a maximum of 0.04% P and a maximum of 0.05% S. The sheet was 0.13 mm (±10%) thick, and the UPC number was 13320(16AS). Magnetite powder, supplied by Alfa Aesar, was CAS 1317-61-9, grain size being less than 325 mesh (44 μm and smaller) with 97% purity. All concentrations are reported in w/w percentages.

2.3. Experimental methodology

Two experimental set-ups were used: a differential reactor (DR) (Fig. 1a) and a bench-scale, fixed-bed reactor (BSFBR) (Fig. 1b). The isothermal DR was loaded with the catalyst pellet and the appropriate gas mixture was fed while the temperature-programmed furnace was heated up. For runs performed with non-pretreated carbon steel, the temperature was raised at the setpoint under Ar gas flow of chromatography purity. Once the operating temperature was reached, the reactant gas mixture was fed to the reactor (6.6% ethanol, 2.2% CO_2 and 91.2% Ar in volume). The reforming test lasted approximately 3 h. The reaction gas was distributed equally among the 5 quartz reaction chambers so that different catalysts could be tested simultaneously under identical conditions (gas flow, pressure, temperature), 1 reactor chamber being kept without catalyst (blank experiment). Gas compositions and flow rates were controlled by rotameters (calibration done by OMEGA). Carbon steel 1008 sheet, of 1.6 mm thickness, was cut into circular pellets, 12.7 mm in diameter, then packed into the inner quartz tubes retained in place by a pad of quartz wool. The inner tubes included porous, fused quartz disks (of coarse porosity, 40–90 μm, and 1.5 cm diameter).

An ethanol vapour/CO_2 gas mixture of molar ratio 3/1 was chosen to maintain an excess of carbon over oxygen aimed at maximizing carbon formation [46,47]. The operating temperature selected, 550 °C, was the theoretical optimal temperature for carbon formation, according to Gibbs energy minimization for ethanol dry reforming calculation and published information regarding the Boudouard reaction on iron [20,41]. The product gases from each reactor cell were sampled alternatively, via a computer-controlled valve assembly (Valco); the recovered gas samples were then directed to the Balzers QMG-420 quadrupole mass spectrometer (QMS) for identification. The QMS was calibrated with pure, standard gases, diluted to appropriate levels in carrier Ar gas. The accuracy of the analysis was ±3%, and reproducibility was ±2%. Since the aim of the work described in this paper was to qualitatively explore the steel catalyst in the reaction studied, full mass and energy balances were not determined. The flow rate was 25 ml/min per tube. The Gas Hourly Space Velocity (GHSV) was 2300 $ml_{gas}\ g_{cata}^{-1}\ h^{-1}$, including Ar, and 250 $ml_{gas}\ g_{cata}^{-1}\ h^{-1}$ without Ar. This low GHSV disguised the fact that the reactants could not reach all of the catalyst mass because the latter was not porous. If the effective surface of the catalyst was considered for the calculation of GHSV ($1.8 \times 10^{-4}\ m^2/g$) instead of catalyst mass, the result was $13.3 \times 10^6\ ml_{gas}\ m^{-2}{}_{cata}\ h^{-1}$ with Ar and $1.4 \times 10^6\ ml_{gas}\ m^{-2}{}_{cata}\ h^{-1}$ without Ar. The calculation was based on the geometrical surface value of the steel, which was $1.8 \times 10^{-4}\ m^2/g$. Treatment of the catalyst prior to the reaction (partial oxidation) enhanced this surface, but was still far too low to be measured precisely.

The BSFBR, also made of quartz, served to reproduce the reaction on a larger scale and obtain mass and energy balances. The BSFBR's internal diameter was 46 mm, and it was 122 cm long. The experimental conditions were 550 °C, 1 atm and no carrier gas. Ethanol was pumped in liquid form (0.33 ml/min) and vaporized in a heated pipe before being mixed with CO_2 (140 ml/min). The 1/1 molar ratio of ethanol/CO_2 favored reforming; steel sheet weight was 24.3 g,

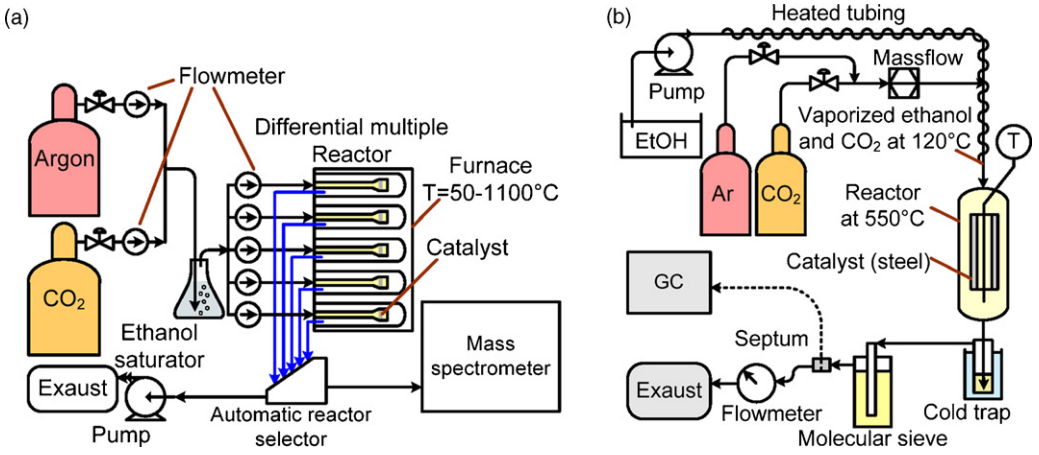

Fig. 1. (a) Differential reactor (DR), and (b) bench-scale, fixed-bed reactor (BSFBR).

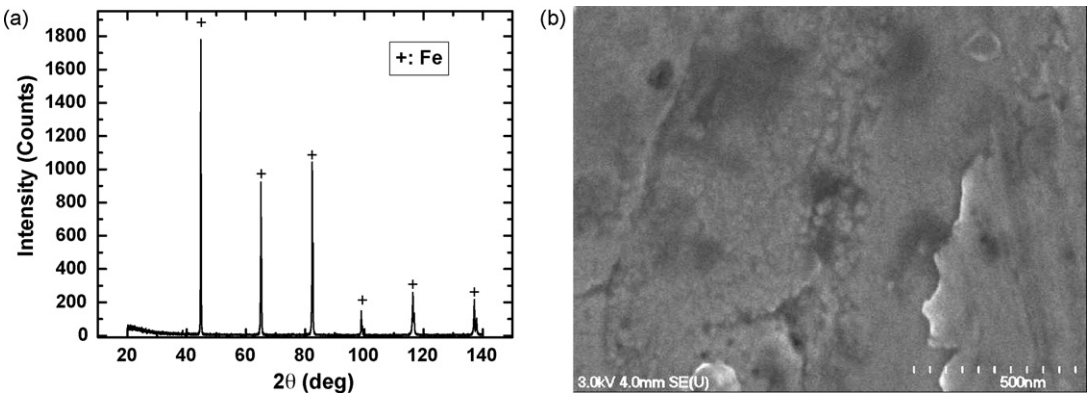

Fig. 2. (a) XRD data, and (b) FEGSEM image of carbon steel 1008 before thermal treatment.

and the GHSV was 2000 $ml_{gas}\,h^{-1}\,g_{cata}{}^{-1}$. As reported previously [46,47], the internal volume of the catalyst was unreachable and so, when only the geometrical surface of the sheet was considered, the GHSV was $1.1 \times 10^6\ ml_{gass}\,m^{-2}{}_{cata}\,h^{-1}$.

The exit gas was dried in a cold trap and molecular sieve column, then analyzed with a Model CP3800 GC from Varian Inc. The catalyst was formed of 4 bands, each 2.54 cm wide, 31 cm long and weighing 24.3 g, fixed to the central thermocouple which was caged in a quartz tube.

2.4. Catalyst characterization

The pictures in Figs. 2–6 were taken with an Hitachi S-4700 FEGSEM. XRD data were obtained by means of a Panalytical X'pert PrO diffractometer and Cu Kα radiation at room temperature, along with instrumental settings of 45 kV and 40 mA, to particularly detect crystalline phases present in the carbon steel catalyst. The Brunauer–Emmett–Teller (BET) adsorption method was employed to measure the specific surface of oxides, this measurement being made at 77 K with a Quantachrome Autoasorb 1, and assuming a 0.162 nm^2 cross-sectional area for N_2.

3. Results and discussion

3.1. Tests with fresh catalyst

In the first tests, we used steel in the as-purchased condition. Its XRD analysis, recorded at ambient temperature, displayed only peaks due to the presence of iron of uniform morphology (Fig. 2a and b). At 550 °C, no reforming or decomposition reaction was observed, and no carbon deposition was detectable. Traces of deposited carbon, visualized by FEGSEM, were found in a rather amorphous, non-organized state, but no CNF or CNT forms were observed. In regard to gaseous products, the result was very similar to the blank test performed at 550 °C and at a flow rate of 25 ml/min (Fig. 3a). The absence of activity was related to the low catalytic activity of the steel in this reaction (Fig. 2). Even if some catalytic activity existed, reaction severity (mainly space velocity and temperature) was not sufficient to generate reforming reactions to a significant extent. Specific surface was not measured by the BET method, but FEGSEM pictures (see surface smoothness in Fig. 2b) clearly showed that there was no internal porosity and that the surface could essentially be measured geometrically; calculation gave a specific surface of the order of 20 cm^2/g.

Space velocity is an important parameter in any catalytic test and, in order to investigate under which conditions the thermal cracking process is possible, 2 experiments were previously performed and reported [46,47], employing the above-described DR set-up. The results of these experiments showed that, for the reforming conditions of our test, in the absence of catalysts, no significant cracking or reforming activity was detectable at a total flow of 25 ml/min per tube, while some activity was observed at a flow rate of 3 ml/min (from the reactor's volume, we calculated a GHSV of 750 and 90 h^{-1}, respectively). Fig. 3, taken from previous publications [46,47], illustrates this point.

3.2. Activation of the catalyst

Thermal treatment was found to be necessary to activate the catalyst of the targeted reaction, principally via improvement of the

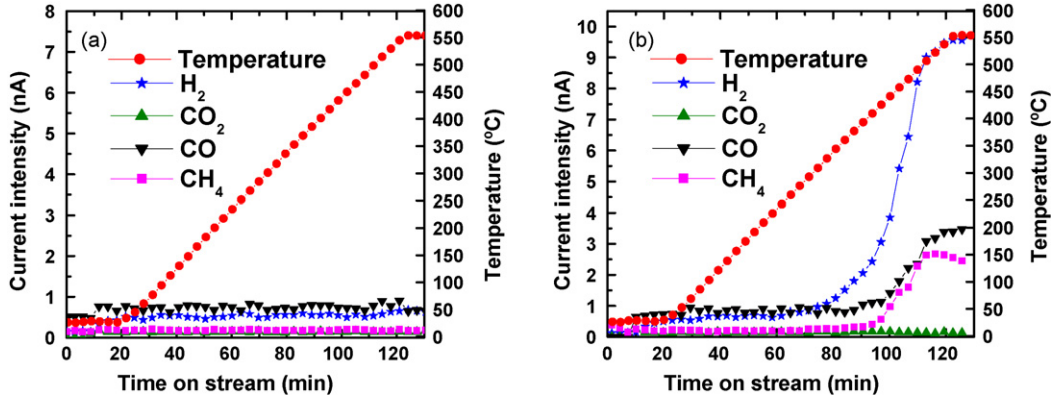

Fig. 3. Product gas of dry reforming at 550 °C with fresh steel as catalyst: (a) no reaction observed at a flow rate of 25 ml/min, and (b) reaction in progress at a flow rate of 3 ml/min (From [46,47]).

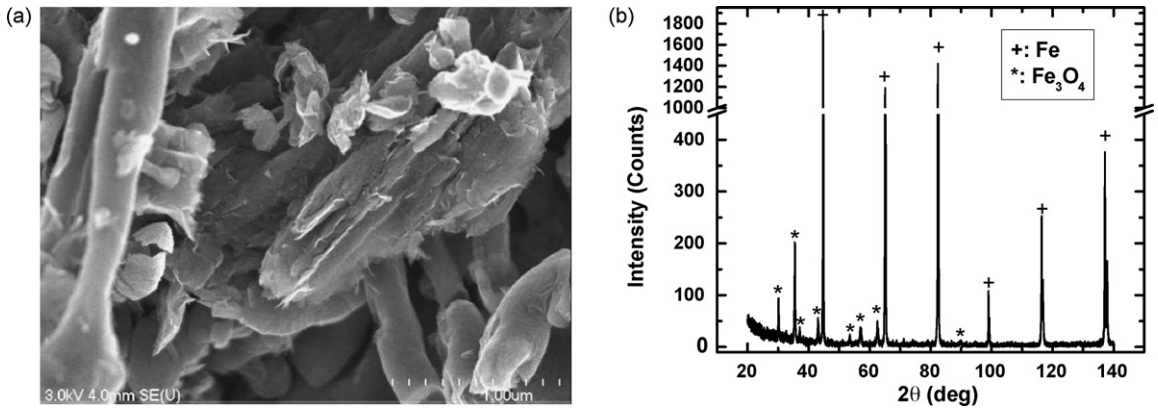

Fig. 4. (a) FEGSEM image, and (b) XRD analysis of the catalyst 1 surface after dry reforming.

specific surface. The protocol of this activation treatment consisted of the following 3 "generic" steps:

Step 1: The steel was heated to 800 °C under a blanket of Ar of chromatographic purity and was kept at this temperature for 1 h.
Step 2: The thus-treated steel was then cooled to 25 °C at a rate of 5 °C/min.
Step 3: The steel from step 2 was exposed to normal air for 24 h.

The so-treated catalyst from step 3 was thus ready for reforming tests at 550 °C in the DR lasting 3 h. The following experimental tests employed 2 catalyst samples which were submitted to "selection" of the above-described 3 generic steps.

Catalyst 1 was not submitted to step 3, but catalyst 2 was. The result was that catalyst 1 was not in contact with oxygen before the reforming test, while catalyst 2 was in contact with atmospheric oxygen at ambient temperature during step 3. Both were tested in the DR.

The results of the reforming tests in the presence of catalyst 1 demonstrated that ethanol decomposition and carbon formation took place at significant levels (see Fig. 4a). However, carbon was not yet apparent in the form of CNF and, consequently, thermal treatment in an inert atmosphere could not account for either the entire catalytic activity during reforming or for the formation of CNF. XRD (Fig. 4b) revealed only iron, but, from the peak heights seen in Figs. 2 and 4a, we concluded that there were changes in the concentration of the iron phases. Some magnetite was detected on the sample, but it was formed after the reforming test, when the catalyst surface was exposed to atmospheric oxygen for the first time.

Catalyst 2 was analyzed by XRD after reaction step 3 (exposure to ambient atmosphere at room temperature). Fig. 5b shows that particles of magnetite ($Fe^{2+}Fe_2^{6+}O_4^{8-}$), confirmed by XRD in Fig. 5a, appeared on the surface of catalyst 2. Magnetite could not be formed during thermal treatment because no oxygen source was available. This mixed oxide component appeared after treatment, and was obviously due to oxidation of the treated surface by ambient air before XRD and FEGSEM analysis. Thus, air oxidized the steel after thermal treatment and not before. In Fig. 4b, the peaks at $2\theta = 65°$ (1000 counts) and 83° (1050 counts) are much higher, compared to the peak at 44° (1800 counts as in Fig. 2b), than they are in Fig. 2a (65° = 1000 counts and 83° = 1050 counts). These variations in relative height are an indication of phase change in the steel, and they might play a role in steel oxidation on exposure to air after treatment.

Catalyst 2 was tested under the same dry reforming conditions over a 3-h period. The extent of the reforming reaction was the same as that found in the previous run with catalyst 1, but the carbon deposit formed was different. CNF, with diameters ranging from 15 to 100 nm, and containing metal particles, were now evident, as illustrated in Fig. 6a. Elemental analysis of the mechanically sampled (through rubbing) carbon revealed a weak iron signal, confirming the role of magnetite in CNF formation. Moreover, as Fig. 5b indicates, the range of carbon filament diameters (from Fig. 6a) was close to the size range of the magnetite particles. XRD analysis (Fig. 6b) disclosed that magnetite was not present at the surface of the catalyst after the reforming test. Cementite, Fe_3C, was the predominant substance detected on the surface. Some iron was also detected, but most of it must have come from internal steel unexposed to the reactants.

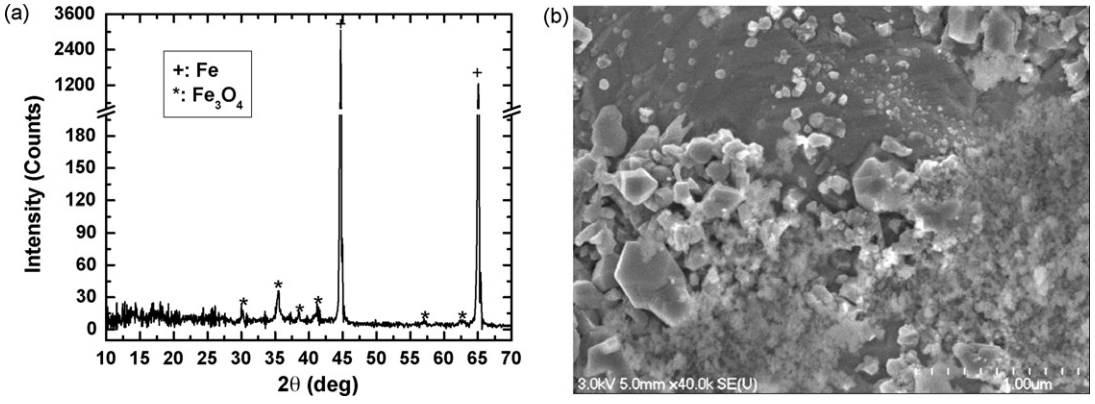

Fig. 5. (a) XRD analysis, and (b) FEGSEM image showing magnetite formed on carbon steel 1008 after thermal treatment at 800 °C for 1 h.

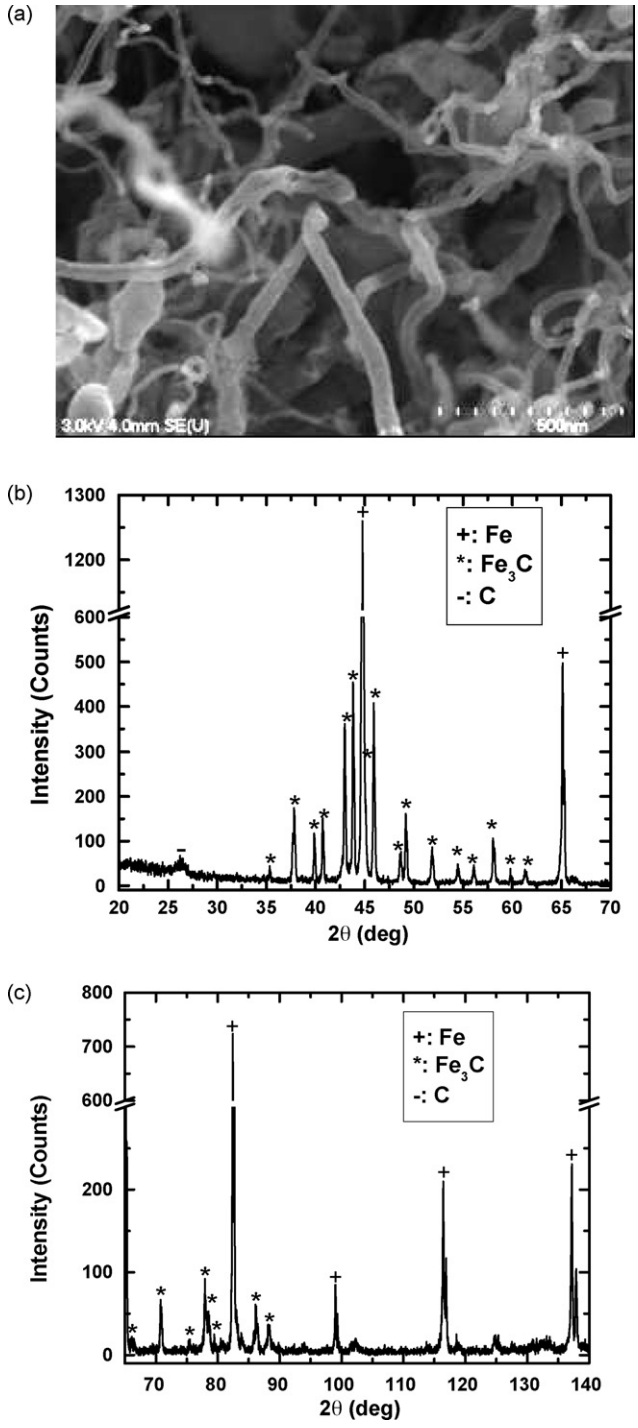

Fig. 6. (a) FEGSEM images, and (b and c) XRD analysis of the catalyst 2 surface after its use in dry reforming.

3.3. Role of magnetite

A 2-h experiment was conducted with shim steel (catalyst 3: treated with the 3 steps, with step 3 shortened to 6 h) installed in the BSFBR. The results reveal that the phenomenon observed in the DR with carbon steel was reproduced in the BSFBR. Fig. 7a displays CNF formation. In addition, the XRD data reported in Fig. 7b demonstrated iron carbide, iron, and graphitic carbon in the sample. However, Fe was not responsible for CNF production because,

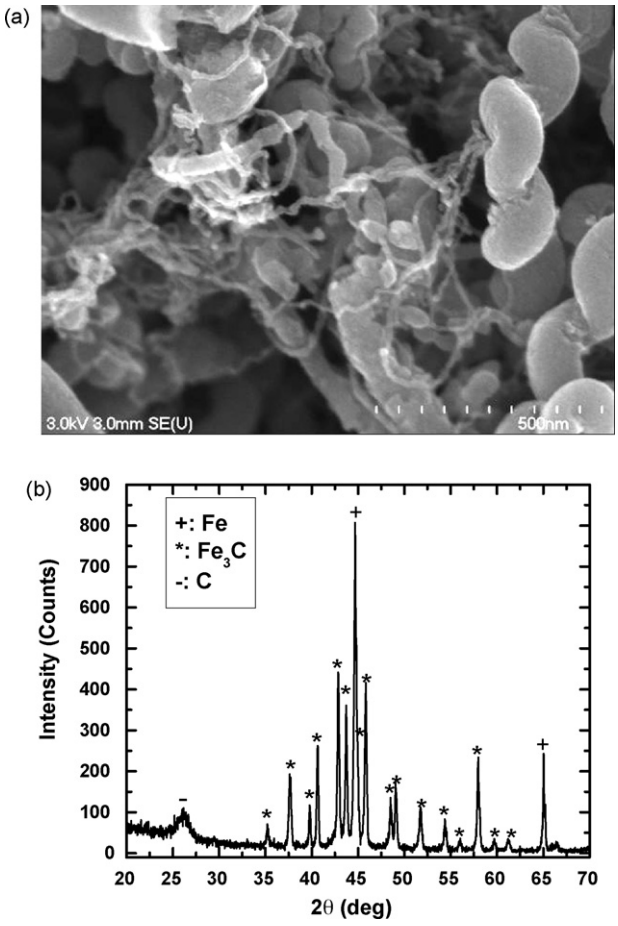

Fig. 7. (a) FEGSEM image, and (b) XRD analysis of shim steel after thermal-oxidative treatment and reforming.

as discerned in previous experiments, it was present in the reaction where the catalyst was not oxidized and no carbon filaments were formed. To better determine which compound was responsible for CNF production, additional experiments were performed.

The first experiment was conducted in the BSFBR, on a second sample of catalyst 3. The reforming test was terminated after 15 min. Subsequent XRD analysis of the catalyst showed that all of the magnetite was consumed (Fig. 8), and that only iron carbide and iron XRD peaks were obtained.

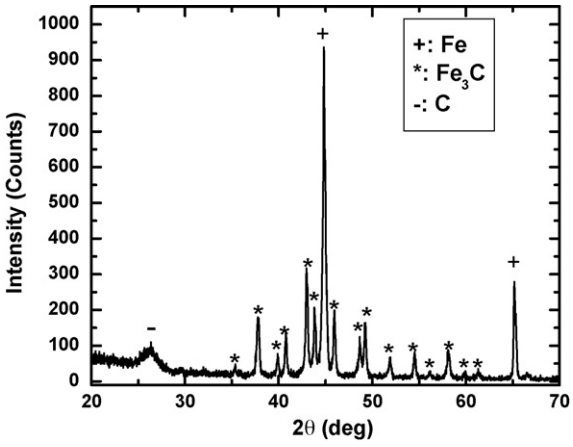

Fig. 8. XRD analysis of treated shim steel after 15 min reforming at 550 °C in the pilot reactor.

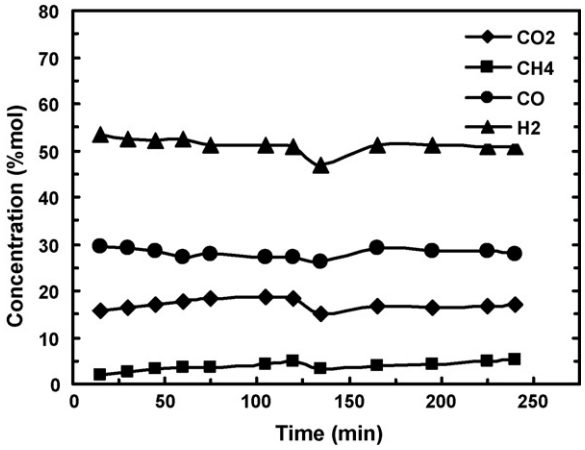

Fig. 9. Gas concentration evolution over time on the treated shim catalyst.

A second test of catalyst 3 was undertaken for 4 h in the same conditions as the previous experiment. Ethanol conversion and CO_2 consumption were 100 and 26%, respectively, and catalyst deactivation was not detected. Fig. 9 shows the evolution of gas product concentration over time, as recorded by GC analysis. The change in H_2 v/v concentrations, from the beginning (53.5%) to the end of the test (51%), was only 2.5%. Variations in concentration of the other gases (CO_2, CO and CH_4) were also below 3%. Since the systematic error of these analyses was typically between 2 and 5%, it can be reasonably concluded that the observed differences were not statistically significant. Average flow out was 611 ml/min. After performing the 4-h reforming test at 550 °C, 12.8 g of carbon was deposited on the catalyst, mainly as CNF. An amount of 5.8 g of water was recovered at the end of the test.

Because of the many parallel and successive reactions occurring during the tests, it was not possible, without an appropriate chemical marker, to calculate the ratio of reformed ethanol over cracked ethanol through mass balance. CO_2 could be used (consumed) by dry reforming and produced from other reactions (i.e., CO disproportionation = Boudouard reaction). On the other hand, the minimal amount of reformed ethanol required to get the obtained result could be directly calculated from the observed CO_2 consumption (0.35 ± 0.05 mol for the whole test). Thus, considering that 1 mol of CO_2 served to reform 1 mol of ethanol, minimum ethanol conversion through dry reforming would be $23 \pm 3\%$. The rest would be either catalytically cracked or reformed.

The last 2 experiments showed that the activity of the catalyst remained high for 4 h despite the absence of magnetite after only 15 min; thus, magnetite's role was only that of igniting the reaction. Since magnetite is possibly an intermediate phase step between iron and iron carbide, it likely catalyzes the reforming reactions but without carbon formation.

3.4. Role of iron carbide

Another experiment was performed to elucidate the role of Fe carbide. Iron carbide was synthesized earlier with pure magnetite powder, H_2 and acetylene (C_2H_2) at 400 °C in the DR. This protocol is already known [54] to produce Fe_3C. XRD analysis showed that all of the magnetite disappeared after only 1 h on stream: thereafter, only iron carbide, Fe_3C, and carbon remained (Fig. 10a). The FEGSEM pictures indicate that magnetite was the precursor of spherical Fe carbide particles (Fig. 10b). The experiment was performed at some excess of carbon (via C_2H_2) to transform all the magnetite to Fe carbide; nevertheless, some carbon was deposited.

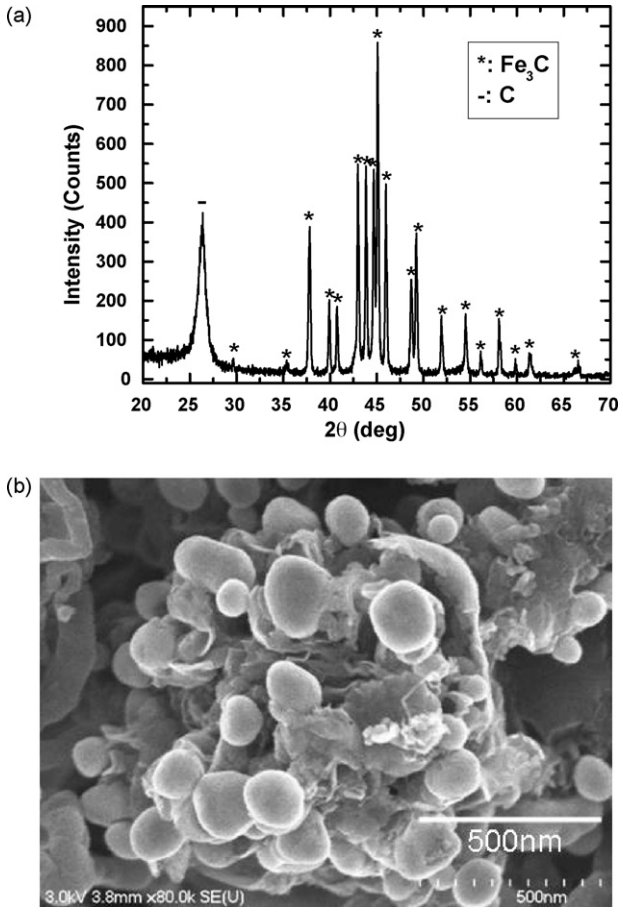

Fig. 10. (a) XRD analysis, and (b) FEGSEM image of particulate iron carbide, produced by treatment of pure magnetite powder with hydrogen and acetylene.

Traces of Fe probably remained but in quantities smaller than the XRD analysis detection limit.

The next step was to conduct the reforming test using the so-produced Fe carbide particles as catalyst. The tests were performed at 550 °C (in the DR) under the same conditions as in the previous tests, with ethanol and CO_2. The FEGSEM picture presented in Fig. 11 shows the presence of CNF grown from Fe carbon particles. This result, combined with previous observations, proves that magnetite is not itself the reforming reaction catalyst and is not responsible for CNF formation; it is, nevertheless, the necessary precursor of Fe carbide particles.

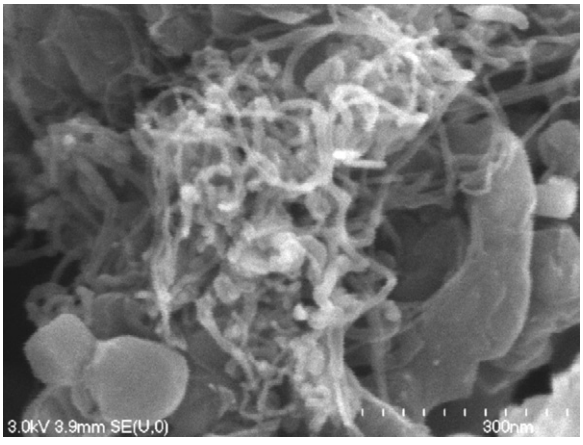

Fig. 11. Filaments produced from acetylene and iron carbide catalyst.

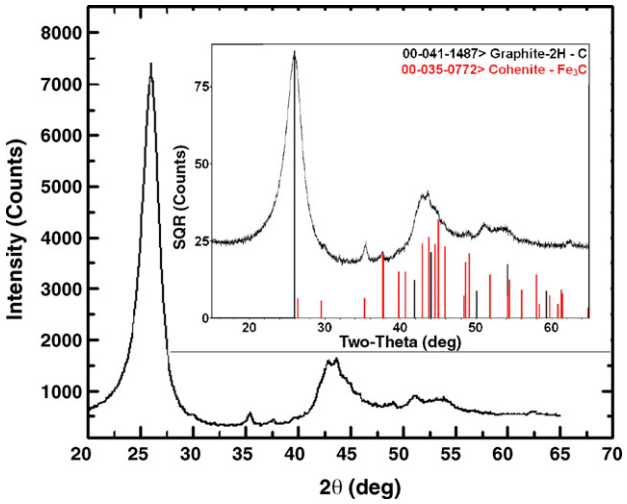

Fig. 12. XRD analysis of CNF produced from shim steel in the pilot reactor.

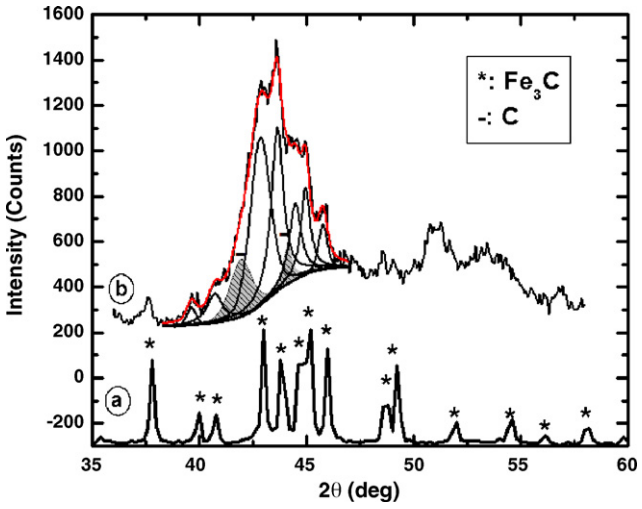

Fig. 13. (a) Iron carbide, produced by the treatment of pure magnetite powder with hydrogen and acetylene, and (b) CNF synthesis from shim steel.

A final experiment was performed to confirm that the Fe carbide phase was the catalyst responsible for CNF formation. CNF so-produced from shim steel in the BSFBR were analyzed by XRD over a period of 1 h, from $2\theta = 20$ to 70°; the results are presented in Fig. 12. Preliminary analysis of the XRD spectra showed that graphitic carbon was the predominant substance in the sample (peak more intense at $2\theta = 26°$), while the main peaks due to the presence of Fe_3C were found in the range of $2\theta = 35$–60°.

To improve the resolution of the iron carbide XRD peaks, a second analysis was undertaken within the range of $2\theta = 35$–60° over a 2-h period. Fig. 13 compares the spectrum recorded for the Fe carbide synthesized from magnetite powder (Fig. 10a) and the deconvoluted spectra of CNF produced from shim steel in the pilot reactor. These results revealed that the broad peak located in the spectrum region between $2\theta = 35$–60° contained all the peaks of Fe carbide and 2 other peaks attributed to the presence of graphitic carbon.

4. Conclusions

This study has demonstrated that a thermally pretreated sheet of common carbon steel is an efficient catalyst in ethanol dry reforming and cracking and that during these reactions produces CNF. Although it was not possible to precisely calculate dry reforming over cracking selectivity of the catalyst, the minimum of ratio "rate of reforming over rate of cracking" was 1/4 in the reaction conditions.

The magnetite particles formed from thermal-oxidative treatment of the catalyst prior to reforming, were quickly reduced by the ethanol cracking or reforming process and were then transformed into Fe_3C via the Boudouard reaction and/or all other carbon-forming reactions (i.e., CH_4 dehydrogenation). Fe_3C particles were active catalysts for CNF production during the cracking or dry (CO_2) reforming of ethanol. Evolution of the product gas concentrations over time showed that the catalyst remained active well after the transformation of all of the magnetite into Fe carbide. Consequently, after magnetite consumption, ethanol continued to react on the Fe carbide particles to produce H_2 and CO, and CNF kept growing in length because of carbon accumulation in the particles. Since FEGSEM disclosed that CNF can contain more than 1 Fe_3C particle, the exact mechanism of the CNF formation process is still not fully understood, and more detailed reaction studies are needed for its elucidation.

Acknowledgements

The authors thank the Natural Sciences and Engineering Research Council of Canada (NSERC) for funding related to this work. Special thanks are due to Mr. Henri Gauvin for his technical assistance, Mrs. Irène Kelsey for characterization of the catalyst, and Mr. Ovid Da Silva for reviewing this manuscript.

References

[1] S. Iijima, Helical microtubules of graphitic carbon, Nature 354 (1991) 56–58.
[2] C. Journet, P. Bernier, Production of carbon nanotubes, Appl. Phys. A: Mater. Sci. Process. 67 (1998) 1–9.
[3] T. Guo, P. Nikolaev, A.G. Rinzler, D.T. Colbert, R.E. Smalley, Self-assembly of tubular fullerenes, J. Phys. Chem. 99 (1995) 10694–10697.
[4] C. Laurent, E. Flahaut, A. Peigney, A. Rousset, Metal nanoparticles for the catalytic synthesis of carbon nanotubes, N. J. Chem. 22 (1998) 1229–1237.
[5] W.K. Hsu, J.P. Hare, M. Terrones, H.W. Kroto, D.R.M. Walton, P.F.J. Harris, Condensed-phase nanotubes, Nature 377 (1995) 687.
[6] W.K. Hsu, M. Terrones, J.P. Hare, H. Terrones, H.W. Kroto, D.R.M. Walton, Electrolytic formation of carbon nanostructures, Chem. Phys. Lett. 262 (1996) 161–166.
[7] D. Laplaze, P. Bernier, W.M. Maser, G. Flamand, T. Guillard, A. Loiseau, Carbon nanotubes: the solar approach, Carbon 36 (1998) 685–688.
[8] M. Terrones, Carbon nanotubes: synthesis and properties, electronic devices and other emerging applications, Int. Mater. Rev. 49 (2004) 325–377.
[9] U. Narkiewicz, N. Guskos, W. Arabczyk, J. Typek, T. Bodziony, W. Konicki, G. Gsiorek, I. Kucharewicz, E.A. Anagnostakis, XRD, TEM and magnetic resonance studies of iron carbide nanoparticle agglomerates in a carbon matrix, Carbon 42 (2004) 1127–1132.
[10] Ch. Emmenegger, P. Mauron, A. Züttel, Ch. Nützenadel, A. Schneuwly, R. Gallay, L. Schlapbach, Carbon nanotube synthesized on metallic substrates, App. Surf. Sci. 162–163 (2000) 452–456.
[11] A. Govindaraj, C.N.R. Rao, Organometallic precursor route to carbon nanotubes, Pure App. Chem. 74 (2002) 1571–1580.
[12] K. Mukul, Z. Xinluo, A. Yoshinori, L. Sumio, S. Maheshwar, H. Kaori, Carbon nanotubes from camphor by catalytic CVD, Mol. Cryst. Liq. Cryst. 387 (2002) 117–121.
[13] N.A. Kiselev, A.V. Krestinin, A.V. Raevskii, O.M. Zhigalina, G.I. Zvereva, M.B. Kislov, V.V. Artemov, Yu.V. Grigoriev, J.L. Hutchison, Extreme-length carbon nanofilaments with single-walled nanotube cores grown by pyrolysis of methane or acetylene, Carbon 44 (2006) 2289–2300.
[14] H.P. Boehm, Carbon from carbon monoxide disproportionation on nickel and iron catalysts: morphological studies and possible growth mechanism, Carbon 11 (1973) 583–586.
[15] R.T.K. Baker, M.A. Barber, P.S. Harris, F.S. Feates, R.J. Waite, Nucleation and growth of carbon deposits from the nickel catalyzed decomposition of acetylene, J. Catal. 26 (1972) 51–62.
[16] R.T.K. Baker, J.R. Waite, Formation of carbonaceous deposits from the platinum-iron catalyzed decomposition of acetylene, J. Catal. 37 (1975) 101–105.
[17] D.K. Liguras, D.I. Kondarides, X.E. Verykios, Production of hydrogen for fuel cells by steam reforming of ethanol over supported noble metal catalysts, Appl. Catal. B 43 (2003) 345–354.

[18] M.C.J. Bradford, M.A. Vannice, CO_2 reforming of CH_4, Catal. Rev.-Sci. Eng. 41 (1999) 1–42.
[19] R.T.K. Baker, P.S. Harris, R.B. Thomas, R.J. Waite, Formation of filamentous carbon from iron-, cobalt-, and chromium-catalyzed decomposition of acetylene, J. Catal. 30 (1973) 86–95.
[20] G.G. Tibbetts, Carbon fibers produced by pyrolysis of natural gas in stainless steel tubes, Appl. Phys. Lett. 42 (1983) 666–668.
[21] A. Sacco, P. Thacker, T. Nan Chang, A.T.S. Chiang, The initiation and growth of filamentous carbon from iron in H_2, CH_4, H_2O, CO_2, and CO gas mixtures, J. Catal. 85 (1983) 224–236.
[22] R.T.K. Baker, P.S. Harris, H.J. Henderson, R.B. Thomas, Formation of carbonaceous deposits from the reaction of methane over nickel, Carbon 13 (1975) 17–22.
[23] W.R. Ruston, M. Warzee, J. Hennaut, J. Waty, The solid reaction products of the catalytic decomposition of carbon monoxide on iron at 550 °C, Carbon 7 (1969) 47–57.
[24] V. Kehrer Jr., H. Leidheiser Jr., The catalytic decomposition of carbon monoxide on large metallic single crystals, J. Phys. Chem. 58 (1954) 550–555.
[25] G.D. Renshaw, C. Roscoe, P.L. Walker, Disproportionation of CO I. Over iron and silicon-iron single crystals, J. Catal. 18 (1970) 164–183.
[26] P.S. Harris, R.T.K. Baker, R.A. Birch, Formation of carbon deposits from decomposition of acetone over nickel, Carbon 11 (1973) 531–539.
[27] N.M. Rodriguez, A review of catalytically grown carbon nanofibers, J. Mater. Res. 8 (1993) 3233–3250.
[28] O.C. Carneiro, P.E. Anderson, N.M. Rodriguez, R.T.K. Baker, Decomposition of CO-H_2 over graphite nanofiber-supported iron and iron-copper catalysts, J. Phys. Chem. B 108 (2004) 13307–13314.
[29] O.C. Carneiro, N.M. Rodriguez, R.T.K. Baker, Growth of carbon nanofibers from the iron-copper catalyzed decomposition of $CO/C_2H_4/H_2$ mixtures, Carbon 43 (2005) 2389–2396.
[30] C. Park, R.T.K. Baker, Carbon deposition on iron-nickel during interaction with ethylene-hydrogen mixtures, J. Catal. 179 (1998) 361–374.
[31] R. Gao, C.D. Tan, R.T.K. Baker, Ethylene hydroformylation on graphite nanofiber supported rhodium catalysts, Catal. Today 65 (2001) 19–29.
[32] R.T.K. Baker, J.J. Chludzinski Jr., N.S. Dudash, A.J. Simoens, The formation of filamentous carbon from decomposition of acetylene over vanadium and molybdenum, Carbon 21 (1983) 463–468.
[33] R.T.K. Baker, J.R. Alonzo, J.A. Dumesic, D.J.C. Yates, Effect of the surface state of iron on filamentous carbon formation, J. Catal. 77 (1982) 74–84.
[34] R.T.K. Baker, M.S. Kim, A. Chambers, C. Park, N.M. Rodriguez, The relationship between metal particle morphology and the structural characteristics of carbon deposits, Stud. Surf. Sci. Catal. 111 (1997) 99–109.
[35] S. Cavallaro, V. Chiodo, A. Vita, S. Freni, Hydrogen production by auto-thermal reforming of ethanol on Rh/Al_2O_3 catalyst, J. Power Sources 123 (2003) 10–16.
[36] C. Diane, H. Idris, A. Kiennemann, Hydrogen production by ethanol reforming over Rh/CeO_2-ZrO_2 catalysts, Catal. Commun. 3 (2002) 565–571.
[37] F. Frusteri, S. Freni, V. Chiodo, L. Sapadaro, G. Bonura, S. Cavallaro, Potassium improved stability of Ni/MgO in the steam reforming of ethanol for the production of hydrogen for MCFC, J. Power Sources 132 (2004) 139–144.
[38] S. Freni, S. Cavallaro, N. Mondello, L. Sapadaro, F. Frusteri, Production of hydrogen for MC fuel cell by steam reforming of ethanol over MgO supported Ni and Co catalysts, Catal. Commun. 4 (2003) 259–268.
[39] F. Marino, M. Boveri, G. Baronetti, M. Laborde, Hydrogen production via catalytic gasification of ethanol. A mechanism proposal over copper-nickel catalysts, Int. J. Hydrogen Energy 29 (2004) 67–71.
[40] F. Haga, T. Nakajima, K. Yamashita, S. Mishima, Effect of crystallite size on the catalysis of alumina-supported cobalt catalyst for steam reforming of ethanol, React. Kinet. Catal. Lett. 63 (1998) 253–259.
[41] J.R. Rostrup-Nielsen, J. Sehested, J.K. Norskov, Hydrogen and synthesis gas by steam- and CO_2 reforming, Adv. Catal. 47 (2002) 65–139.
[42] U.C. Chung, W.S. Chung, Mechanism on growth of carbon nanotubes using CO-H2 gas mixture, in: PRICM 5: The Fifth Pacific Rim International Conference on Advanced Materials and Processing, 475–479, 2005, pp. 3551–3554.
[43] R.Y. Chen, W.Y.D. Yeun, Review of the high-temperature oxidation of iron and carbon steels in air or oxygen, Oxid. Met. 59 (2003) 433–468.
[44] C.X. Pan, Y.L. Liu, F. Cao, J.B. Wang, Y.Y. Ren, Synthesis and growth mechanism of carbon nanotubes and nanofibers from ethanol flames, Micron 35 (2004) 461–468.
[45] K. De Oliveira-Vigier, N. Abatzoglou, F. Gitzhofer, Dry-reforming of ethanol in the presence of a 316 stainless steel catalyst, Can. J. Chem. Eng. 83 (2005) 978–984.
[46] N. Abatzoglou, J. Blanchard, H. Oudghiri-Hassani, S. Jankhah, F. Gitzhofer, The DRIVE2 process for carbon sequestration through dry reforming of ethanol using iron catalysts, WSEAS Trans. Environ. Dev. 2 (2006) 15–21.
[47] N. Abatzoglou, J. Blanchard, H. Oudghiri-Hassani, S. Jankhah, F. Gitzhofer, The use of catalytic reforming reactions for CO_2 sequestration as carbon nanotubes, in: WSEAS International Conference on Energy & Environmental Systems Proceedings, 2006, pp. 21–26.
[48] H.T. Abuluwefa, R.I.L. Guthrie, F. Ajersch, Oxidation of low carbon steel in multicomponent gases: Part I. Reaction mechanisms during isothermal oxidation, Metall. Mater. Trans. A 28A (1997) 1633–1641.
[49] R.Y. Chen, W.Y.D. Yuen, Oxidation of low-carbon, low-silicon mild steel at 450–900 °C under conditions relevant to hot-strip processing, Oxid. Met. 57 (2002) 53–79.
[50] H.T. Abuluwefa, R.I.L. Guthrie, F. Ajersch, Oxidation of low carbon steel in multicomponent gases: Part II. Reaction mechanisms during reheating, Metall. Mater. Trans. A 28A (1997) 1643–1651.
[51] D. Caplan, G.I. Sproule, R.J. Hussey, M.J. Graham, Oxidation of Fe-C alloys at 500 °C, Oxid. Met. 12 (1978) 67–82.
[52] S. Jankhah, N. Abatzoglou, F. Gitzhofer, J. Blanchard, H. Oudghiri-Hassani, Catalytic properties of carbon nano-filaments produced by iron-catalyzed reforming of ethanol, Chem. Eng. J. 139 (2008) 532–539.
[53] J.R. Fox, F.A. Pesa, B.S. Curatolo, and Standard Oil Co., USA, Process for reforming alcohols. Patent US 1983-531965 (1986) 1–4.
[54] N. Guskos, E.A. Anagnostakis, V. Likodimos, T. Bodziony, J. Typek, M. Maryniak, U. Narkiewicz, I. Kucharewicz, S. Waplak, Ferromagnetic resonance and ac conductivity of a polymer composite of Fe_3O_4 and Fe_3C nanoparticles dispersed in a graphite matrix, J. Appl. Phys. 97 (2005), 024304-1-024304-6.